

FAR-IR AND RADIO THERMAL CONTINUA IN SOLAR FLARES

J. KAŠPAROVÁ¹, P. HEINZEL¹, M. KARLICKÝ¹, Z. MORAVEC²
and M. VARADY^{2,1}

¹*Astronomický ústav Akademie věd České republiky, v.v.i., Fričova 298,
251 65 Ondřejov, Czech Republic*

²*Katedra fyziky, Universita J. E. Purkyně, České mládeže 8,
400 24 Ústí nad Labem, Czech Republic*

Abstract. With the invention of new far-infrared (FIR) and radio mm and sub-mm instruments (DESIR on SMESE satellite, ESO-ALMA), there is a growing interest in observations and analysis of solar flares in this so far unexplored wavelength region. Two principal radiation mechanisms play a role: the synchrotron emission due to accelerated particle beams moving in the magnetic field and the thermal emission due to the energy deposit in the lower atmospheric layers. In this contribution we explore the time-dependent effects of beams on thermal FIR and radio continua. We show how and where these continua are formed in the presence of time dependent beam heating and non-thermal excitation/ionisation of the chromospheric hydrogen plasma.

Key words: solar flares, radiative hydrodynamics, continuum emission

1. Introduction

New ground-based and space-borne instruments are being designed to observe the Sun in so-far unexplored wavelength windows or with unprecedented spatial and/or temporal resolution. Here we are motivated by the planned observations of solar flares in far infrared (FIR) region and in sub-millimetre/millimetre (SMM) radio wavelengths. A specific FIR window where the radiation is not observable from the Earth is between 35 and 250 μm and this is expected to be explored by the DESIR telescope on board the SMESE satellite (SMall Explorer for Solar Eruptions – Vial et al. (2007)). At SMM wavelengths, observations were already performed by Kaufmann et al. (2000) and Lüthi et al. (2004). However, new data are expected soon from ALMA (Atacama Large Millimeter Array) radio-interferometer.

In both FIR and SMM domains a superposition of two radiation components is expected: the high-frequency part of the microwave spectrum from ultra-relativistic electrons and/or positrons (non-thermal synchrotron emission) and the low-frequency part of the thermal flare continuum. As suggested in Vial et al. (2007), these emissions provide, respectively, a unique diagnostic of the non-thermal particles (beams) and of the thermal response of the lower flare atmosphere to the energy deposit. In FIR domain, the relative importance of both processes was estimated by Ohki and Hudson (1975). Recently, Loukitcheva et al. (2004) and Heinzel and Avrett (2009) computed the microwave thermal continua formed in dynamic and static semi-empirical atmospheres, respectively.

In this study, we concentrate on formation of such thermal emission in the $35 \mu\text{m} - 1 \text{ cm}$ wavelength range originating in a highly dynamical flare atmosphere heated by short-duration electron beam pulses. Section 2 describes the mechanisms responsible for the thermal emission, characteristics of the emission corresponding to simulations of the beam heated atmosphere are presented in Section 3. Section 4 summarises our results.

2. Mechanisms of the FIR and SMM thermal continuum formation

Depending on the wavelength, various atmospheric depths can contribute to the emergent FIR and SMM intensity (Heinzel and Avrett, 2009). In the chromosphere, the dominant source of opacity is the hydrogen free-free continuum. The absorption coefficient is given as (Rybicki and Lightman, 1979)

$$\kappa_{\nu}(\text{H}) = 3.7 \times 10^8 T^{-1/2} n_e n_p \nu^{-3} g_{\text{ff}} \quad (1)$$

where n_e and n_p are the electron and proton densities, respectively, T is the temperature, and $g_{\text{ff}} \approx 1$ is the Gaunt factor. At lower temperatures, around the temperature minimum region, H^- free-free opacity plays an important role. The H^- absorption is (Kurucz, 1970)

$$\kappa_{\nu}(\text{H}^-) = \frac{n_e n_{\text{H}}}{\nu} (1.3727 \times 10^{-25} + (4.3748 \times 10^{-10} - 2.5993 \times 10^{-7} / T) / \nu) \quad (2)$$

where n_{H} is the neutral hydrogen density. Total absorption corrected for stimulated emission is then

$$\kappa_{\nu} = [\kappa_{\nu}(\text{H}) + \kappa_{\nu}(\text{H}^-)] (1 - e^{-h\nu/kT}), \quad (3)$$

where h and k are the Planck and Boltzmann constants, respectively. The source function for these free-free processes is the Planck function B_ν . However, the absorption has to be evaluated using number densities coming from non-LTE calculations. Finally, emergent intensity I_ν can be obtained as

$$I_\nu = \int \eta_\nu e^{-\tau_\nu} dz \quad \eta_\nu = \kappa_\nu B_\nu \quad d\tau_\nu = -\kappa_\nu dz, \quad (4)$$

where z is the geometrical height.

3. Flare models

We have evaluated the FIR and SMM continuum emission for non-LTE radiative hydrodynamic models which describe the atmospheric response to the time dependent electron beam heating. In these simulations electron beams of a varying beam flux and power-law spectra are injected into a loop which corresponds to an initially hydrostatic VAL C atmosphere (Vernazza et al., 1981). Then, the time evolution of the beam particles and plasma properties are followed. We also consider the so-called non-thermal collisional rates, C^{nt} , which account for the changes of the atomic level populations due to the collisions with the beams. For more details on the models see Varady et al. (2005); Kašparová et al. (2009).

3.1. TIME VARIATION

Our simulations show that the continuum emission is well correlated with the beam flux on the time scale of the beam flux variation, e.g. on a sub-second time scale. Longer wavelengths (1 cm) exhibit larger relative intensity increase than shorter wavelengths (35 μm) when compared to the preflare (VAL C) intensities – see Figure 1. Furthermore, emission in the $\lambda < 0.2$ mm range depends also on the beam parameters, i.e. the power-law index and the beam flux. Generally, maxima of the emission lag behind the beam flux maxima, the time lag lies within the 0.1 – 0.3 s interval for present simulations.

3.2. INFLUENCE OF NON-THERMAL COLLISIONAL RATES

Although the non-thermal rates can significantly affect the hydrogen level populations and electron densities in some atmospheric layers (Kašparová et al.,

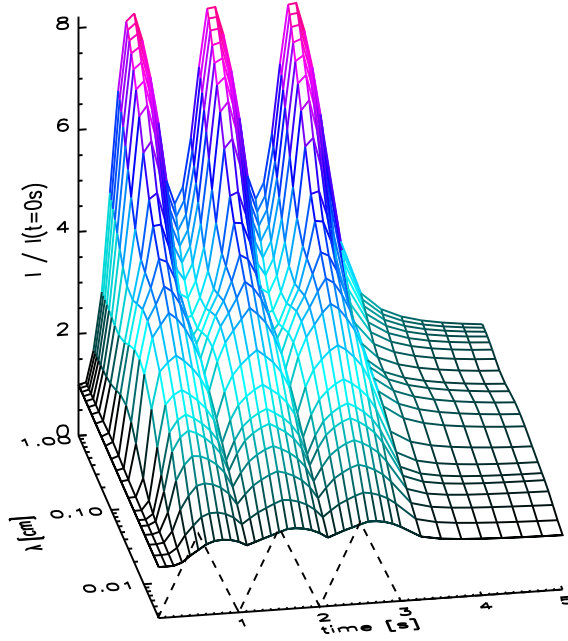


Figure 1: Time evolution of relative continuum intensities scaled to the intensity at $t = 0$ s, i. e. of the VAL C atmosphere, for an electron beam of a power-law index $\delta = 3$ and a maximum beam flux $F_{\max} = 6 \times 10^{10} \text{ erg cm}^{-2} \text{ s}^{-1}$. The dashed line indicates the beam flux time variation.

2005), their influence on FIR and SMM continuum emission is almost negligible. C^{nt} cause only moderate and temporary increase of the continuum intensity shortly after the beam injection into the VAL C atmosphere. Additionally, influence of C^{nt} for $\lambda < 0.2$ mm depends on the beam parameters and it is modulated by the beam flux time variation – see Figure 2.

3.3. FORMATION DEPTHS

Atmospheric layers which contribute the most to the outgoing intensity, i.e. the formation depths, can be understood in terms of the so-called contribution function CF

$$CF = \eta_{\nu} e^{-\tau_{\nu}} \quad I_{\nu} = \int CF \, dz, \quad (5)$$

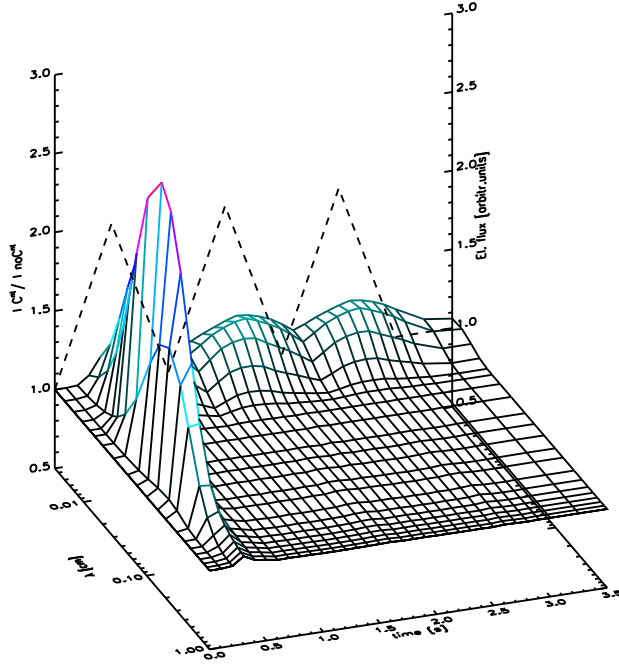


Figure 2: Influence of the non-thermal collisional rates C^{nt} . The plot shows the ratio of intensities with and without C^{nt} . The dashed line indicates the beam flux time variation. The beam parameters are the same as in Fig. 1. Note the reversed wavelength scale with regard to Figure 1.

compare with Eq. (4). In the initial atmosphere, emission at wavelengths shorter than $\lambda \approx 1$ mm comes from deep, photospheric layers, whereas the continuum at other wavelengths is formed at the upper part of the atmosphere. However, as the atmosphere is heated by the beams, the emission is formed mainly at the chromospheric heights (above $z \approx 1000$ km). The emission which comes from these layers can be influenced also by C^{nt} since the beams deposit their energy there. On the other hand, the emission in the $35 - 200 \mu\text{m}$ range partially originates from the photosphere – see Figure 3.

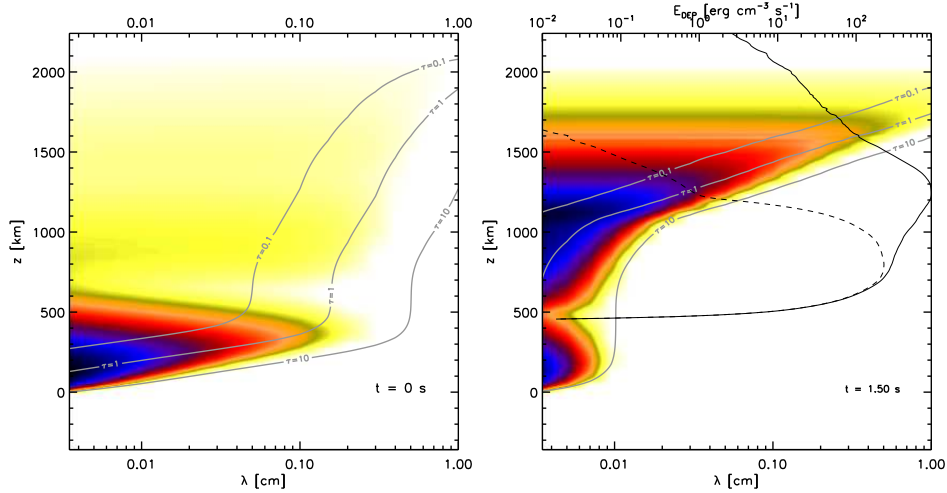


Figure 3: An example of the time evolution of contribution function CF (Eq. 5) for an electron beam of $\delta = 3$ and $F_{\max} = 4.5 \times 10^{10} \text{ erg cm}^{-2} \text{ s}^{-1}$. *Left:* CF for the VAL C atmosphere, i.e. at $t = 0 \text{ s}$. *Right:* CF at $t = 1.5 \text{ s}$ corresponding to the model with included C^{nt} . Colour scale going from white to black represents the range of $\log CF$ values (from minimum to maximum). Black solid curve indicates the total energy deposit of the beam, dashed curve is for the energy deposit on hydrogen E_{H} . C^{nt} are proportional to E_{H} , therefore the dashed line marks the layers which are affected by C^{nt} . Gray lines display the levels of optical depth $\tau = 0.1, 1, 10$.

4. Conclusions

Using the results of non-LTE radiative hydrodynamic simulations we have found that the rapidly varying beam flux can manifest itself in the thermal FIR and SMM continuum intensities. We show that the continuum intensities do vary on the beam flux variation time scales. However, the direct influence of the beam electrons via the non-thermal collision is moderate only. The emission is mainly affected by the temperature variations which result from the time dependent heating by the beams. Concerning the formation of the emission, in the heated atmosphere or due to the non-thermal collisions the continua are formed in the upper atmosphere. The intensities in the $35 - 200 \mu\text{m}$ partially originate also from the photosphere.

In this work we did not consider effects related to the situation when the frequency of the emitted electromagnetic waves is close to the local plasma

frequency. In the case of the solar atmosphere plasma, these effects must be taken into account at the radio frequency range. We will address this issue for the FIR and SMM emission in a future study.

Acknowledgements

We acknowledge grants 205/04/0358, 205/06/P135, 205/07/1100 (GA CR) and the research project AV0Z10030501 (Astronomický ústav). The non-LTE radiative hydrodynamic simulations were performed on OCAS (Ondřejov Cluster for Astrophysical Simulations) and Enputron, a computer cluster for extensive computations (Universita J. E. Purkyně).

References

- Heinzel, P., and Avrett, E. H.: 2009, *Astrophys. J.*, in preparation .
- Kaufmann, P., Costa, J. E. R., Correia, E., Giménez de Castro, C. G., Raulin, J.-P., and Silva, A. V. R.: 2000, in R. Ramaty, and N. Mandzhavidze (eds), *High Energy Solar Physics Workshop - Anticipating Hessi*, Vol. 206 of *Astronomical Society of the Pacific Conference Series*, p. 318.
- Kašparová, J., Varady, M., Heinzel, P., Karlický, M., and Moravec, Z.: 2009, *Astron. Astrophys.*, submitted .
- Kašparová, J., Varady, M., Karlický, M., Moravec, Z., and Heinzel, P.: 2005, in D. Danesy, S. Poedts, A. De Groof, and J. Andries. (eds), *ESA SP-600: The Dynamic Sun: Challenges for Theory and Observations*, ESA Publication Division. published on CDROM.
- Kurucz, R. L.: 1970, *SAO Special Report* **309**.
- Loukitcheva, M., Solanki, S. K., Carlsson, M., and Stein, R. F.: 2004, *Astron. Astrophys.* **419**, 747–756.
- Lüthi, T., Magun, A., and Miller, M.: 2004, *Astron. Astrophys.* **415**, 1123–1132.
- Ohki, K., and Hudson, H. S.: 1975, *Sol. Phys.* **43**, 405–414.
- Rybicki, G. B., and Lightman, A. P.: 1979, *Radiative processes in astrophysics*, New York, Wiley-Interscience, 1979. 393 p.
- Varady, M., Kašparová, J., Karlický, M., Heinzel, P., and Moravec, Z.: 2005, *Hvar Observatory Bulletin* **29**, 167–176.
- Vernazza, J. E., Avrett, E. H., and Loeser, R.: 1981, *Astrophys. J., Suppl. Ser.* **45**, 635–725.
- Vial, J.-C., Auchère, F., Chang, J., Fang, C., Gan, W. Q., Klein, K.-L., Prado, J.-Y., Trottet, G., Wang, C., and Yan, Y. H.: 2007, *Advances in Space Research* **40**, 1787–1801.